Advanced Physical Research
Vol.5, No.2, 2023, pp.61-72

THE DEPENDENCE OF EXCITON ENERGY LEVELS ON EXTERNAL ELECTRIC FIELD AND CHARGE DOPING IN 2D MATERIALS: AN AB INITIO STUDY

Tran Tuan-Anh*

Department of Physics, Ho Chi Minh City University of Technology and Education,
Ho Chi Minh City, Vietnam

Abstract. This report explores the impact of external electric fields and charge doping on the energy levels of exciton insulators (discovered in AB-bilayer graphene) and exciton transitions (found in bilayer transition metal dichalcogenides structures, denoted as 2D-TMDCs). The results indicate that graphene bilayer materials' exciton insulator energy level is significantly influenced by electron doping and external electric fields, which leads to a broadening of the band gap. By contrast, the band gap in 2D-TMDC bilayer materials narrows when subjected to similar conditions. These findings could be useful in developing electronic devices capable of modifying band gaps with electric fields or charge doping.

Keywords: *2D material, exciton, external electric field, density functional theory.*

Corresponding Author: *Tran Tuan-Anh, Faculty of Applied Sciences, Ho Chi Minh City University of Technology and Education, Ho Chi Minh City, 700000, Vietnam. e-mail: anhtt@hcmute.edu.vn*

Received: *12 January 2023;* ***Accepted:*** *18 April 2023;* ***Published:*** *23 June 2023.*

1. Introduction

An exciton is a bosonic entity formed through the Coulombic interaction between an electron and a hole, much like the way in which an electron and a proton bond to create a hydrogen atom (Kittel, 1996). In the context of contemporary solid-state physics, one exciton is formed through the combination of two fermions, i.e., electrons and holes. Even though some may not accept holes as matter particles, they are a legitimate conserved quantity that arises from the motion of electrons) (Moskalenko & Snoke, 2000). The exciton has an integer spin since each of its constituents, electron and hole, has a half-integer spin. Exciton formation necessitates appropriate conditions, notably the existence of Coulomb forces between an electron and a hole. Excitons come to an end when hole-electron recombination occurs, which is known as exciton lifetime. The average lifetime depends on the substance and conditions. It ranges from several tens of nanoseconds in 2D materials (Palummu *et al*., 2015). Due to the mutual exclusion of electrons and holes, exciton creation is hindered in metals. Contrarily, excitons frequently occur in semiconductors and dielectrics when a sufficient energy photon facilitates their creation by providing strong-enough Coulomb forces (Azhikodan *et al*., 2016). Excitons in oblique semiconductors that exist in other waveguide bands tend to destabilize and break down into free electrons and holes because of a direct band gap structure. The disappearance of an exciton is distinct from electron-hole recombination (Kittel, 1996).

How to cite (APA): Tran, T.A. (2023). The dependence of exciton energy levels on external electric field and charge doping in 2D materials: an AB initio study. *Advanced Physical Research, 5*(2), 61-72.

The dimensions of an exciton are contingent upon its specific classification and can vary from a few angstroms to several hundred angstroms. Excitons can be generally categorized into two varieties based on their dimensions, per the findings outlined in the reference (Moskalenko & Snoke, 2000). A Frenkel exciton is firmly fixed within a lattice cell and relatively minuscule in size, earning its appellation from its discoverer, Frenkel J.Y. (Frenkel, 1931). A flawless Frenkel exciton would adhere to the motion of excitonic waves in the crystal while maintaining electron proximity to the hole (Kittel, 1996). The Frenkel exciton model delineates those that are tightly bounded and diminutive in size. By contrast, the Wannier-Mott exciton, also referred to as the Wannier exciton, is a larger breed of exciton that spans a multitude of lattice cells, with a feeble Coulomb force that distinguishes it from others. This class of exciton is named after the stud (Wannier, 1937) and was first mentioned in works by (Mott & Littleton, 1938), and is exceedingly common in the majority of semiconductors. The present discourse, dealing with the topic of 2D materials, chiefly addresses the Wannier-Mott exciton.

Under normal conditions, the exciton energy spectrum is rarely observed due to its location within the band gap and close proximity to the lower edge of the conduction band (Kittel, 1996). However, the presence of an external field, such as an electromagnetic field, sharpens the spectrum (Edelstein *et al.*, 1989). Consequently, applying a suitable electromagnetic field can alter the binding energy of the exciton, allowing for easier observation of the energy spectrum (Butov, 2001; Elliott & Loudon, 1960).

In the structure of a 2D material, excitonic condensation may alter certain properties that affect its energy structure. Such condensation comes in two forms. In cases where the magnitude of the exciton's binding energy is less than the band gap, no modification of the band gap transpires. However, when the binding energy exceeds the band gap, the exciton's energy range widens, causing the expansion of the default distance between the band gap and valence band. Consequently, the valence band's top and the band gap's bottom are pushed apart, allowing the creation of excitonic insulators, commonly known as excitonium (Werdehausen *et al.*, 2018). The formation of a hetero-bilayer structure by combining two monolayers of different materials generates excitonic transitions or interlayer excitons. This brings about an excitonic interaction shift, reorienting the material's band gap and energy band structure (Fang *et al*, 2014).

The current state of the scientific literature indicates an absence of investigations into the specific structure of excitons in 2D materials, including the spatial arrangement of electrons and holes. Furthermore, there is a lack of comprehensive analyses of the impact of charge doping on exciton energy levels and a lack of systematic studies on the relationship between exciton energy levels and the band gap of low-dimensional materials. Consequently, the present study endeavors to investigate two distinct forms of excitons, namely exciton insulators within graphene bilayer materials and exciton transition within hetero-bilayer materials. Additionally, our research aims to examine the modifications in the band structure, commonly referred to as the energy levels of the exciton, which arise due to the influence of external electric fields and charge doping.

2. Computational method

In this study, the density functional theory (DFT) is employed for ab initio simulations, using the QUANTUM ESPRESSO package (Giannozzi, 2009). To consider electronic-ion core interactions in the simulations, the projector-augmented wave pseudo-potential method (Blöchl, 1994) with an energy cutoff of 60 Ry is used. For the

approximation of the exchange-correlation functions, the generalized gradient approximation with the Perdew, Burke, and Ernzerhof (PBE) parameterization (Perdew *et al*., 1996) is utilized. The van der Waals forces between interlayers are treated using the correction developed by the Thonhauser group (Thonhauser *et al*., 2007). The Brillouin zone is sampled using a (40 × 40 × 1) k-grid mesh based on the Monkhorst–Pack scheme (Monkhorst & Pack, 1976). Energy and force convergence thresholds are set to be 10^{-7} eV and 10^{-6} eV.Å^{-1}, respectively, to reduce interactions between periodic images in adjacent cells. To minimize these interactions, a vacuum spacing of 24 Å is inserted along the vertical direction of the examined materials. Additionally, an electric field, with the negative electric field direction along the z-axis, is applied perpendicularly to the 2D plane of the material. Charge doping involves the application of a total charge to the system (a total charge equal to +1 implies one missing electron from the unit cell, while -1 implies one additional electron on the unit cell).

3. Results and discussions

3.1. Exciton insulators in bilayer graphene

First, we conduct a computation to acquire results for monolayer graphene, a fundamental and well-known material, while excluding any external stimuli. Our investigation yields an optimized graphene structure that exhibited a C-C bond distance of 1.4216 Å, which is consistent with experimental observations (Zhen & Zhu, 2018). The created energy band structure of monolayer graphene is visually represented in Figure 1.a, and the outcomes indicate an absence of a forbidden gap, with the interconnecting of conduction and valence bands at the K point in the reciprocal lattice. The results displayed in Figure 1.*a* are highly predictable and expected. Furthermore, comparable outcomes have been computed and deduced by other scientific groups individually (Torbatian & Asgari, 2018; Wang *et al*., 2018).

After completing the examination of the monolayer graphene material, we proceed to investigate the properties of two-layer graphene, known as bilayer graphene or bi-graphene, in both AA-stacking (bi-graphene-AA) and AB-stacking (bi-graphene-AB) arrangements. Our methodology replicates the optimum conditions of the monolayer graphene assessment. The computation results are presented in Figure 1.*b* and Figure 1.*c*, where the intersection of the two distinct areas still appears at the K point, and the forbidden band is not yet visible. These findings are coherent with observations documented by other research teams (Torbatian & Asgari, 2018), (Wang *et al*., 2014). However, these conclusions only hold true in the absence of external impact, making graphene unsuitable for semiconductor technology. Therefore, we deem it necessary to account for these influences on the material structure to obtain fresh outcomes. After scrutinizing recent studies (Raza & Kan, 2009; Sahu *et al.*, 2016; Wang *et al*., 2018), we resolved to subject AB-bilayer graphene material to an external electric field.

An evaluation is carried out on AB-bilayer graphene material, using two different electric field magnitudes of 0.004 au and 0.008 au, which were converted to 2.057 V/nm and 4.114 V/nm, respectively. The energy band structure and projected density of states (PDOS) results of AB-bilayer graphene are represented in Figures 2.a and 2.b, respectively.

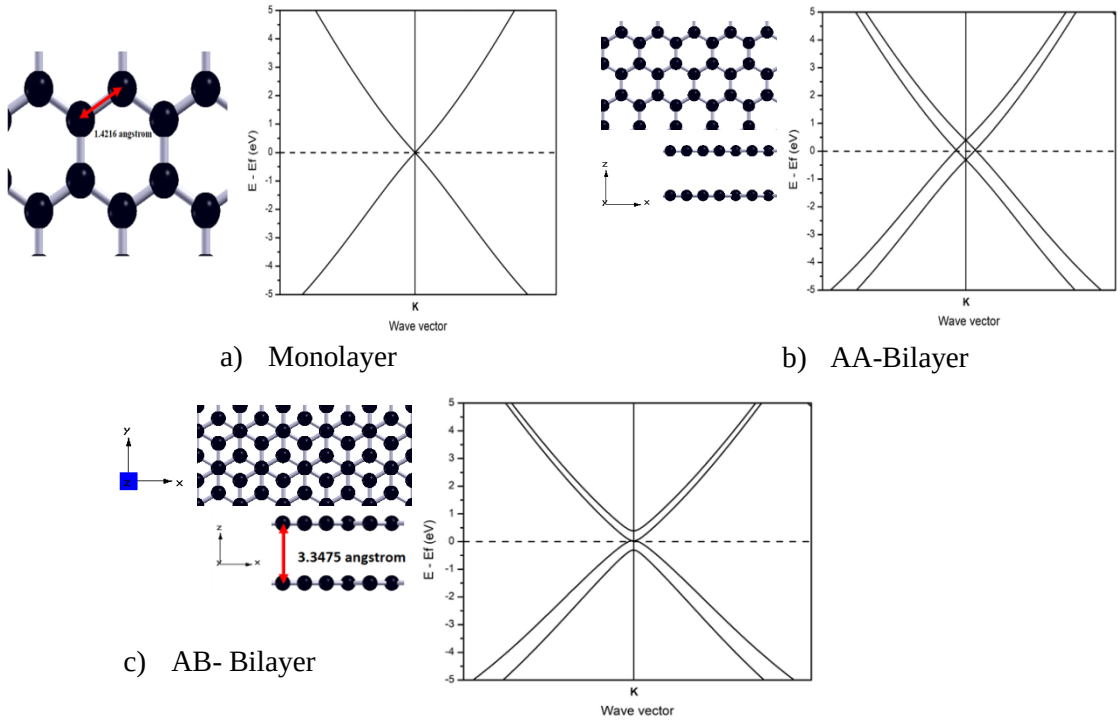

Fig.1. Crystal structure and band structure of graphene *a*) monolayer, *b*) AA-bilayer and *c*) AB-bilayer

As the AB-bilayer graphene material is exposed to external electric fields, a band gap emerges at the K point. At 2.057 V/nm, the band gap is 0.1640 eV, while at 4.114 V/nm, the band gap size increases to 0.2345 eV. It can be inferred that larger external electric fields generate larger band gaps. It should be noted that recently, Rui-Ning Wang's research group in 2016 (Wang *et al.*, 2016) also calculated the band gap sizes at the electric field of 2 V/nm and 4 V/nm, and showed that they were 0.1658 eV and 0.2478 eV, respectively. These results were close to ours, indicating adequate reliability of our findings.

The PDOS peak around the Fermi level displays notable differences. In the case of low electric field, the top of the band structure at point K is tall and narrow (Fig. 2. *a*); meanwhile, it is broad and low for higher electric field (Fig. 2. *b*). This distinction can be explained by the width of the bottom of the conduction band and the top of the valence band for the 4.114 V/nm electric field case, as the loads are evenly distributed, leading to a broadly distributed PDOS. On the other hand, for the lower electric field of 2.057 V/nm, carriers tend to crowd in, leading to much higher density, suggesting the existence of an excitonic insulator.

In order to understand the effect of changing electric field on the band gap, it is necessary to revisit the formula for electron energy at the K point. This formula is represented as follows (Kittel, 1996):

$$E(k) = E_0 + \frac{\hbar^2 k^2}{2m*}$$

where E_0 denotes the fundamental energy level, ħ represents Planck's constant, k denotes the momentum of waves, and all three variables are restricted to fixed values of wave vector. The effective mass, $m*$, is the only variable. As the energy of electrons in the

system increases with an increase in the electric field, E(k) also rises, leading to a decrease in the value of m*. This decrease in the effective mass leads to an increase in the binding energy of excitons, causing the widening of the band gap. As a result, with an increase in electric field, the band gap also increases.

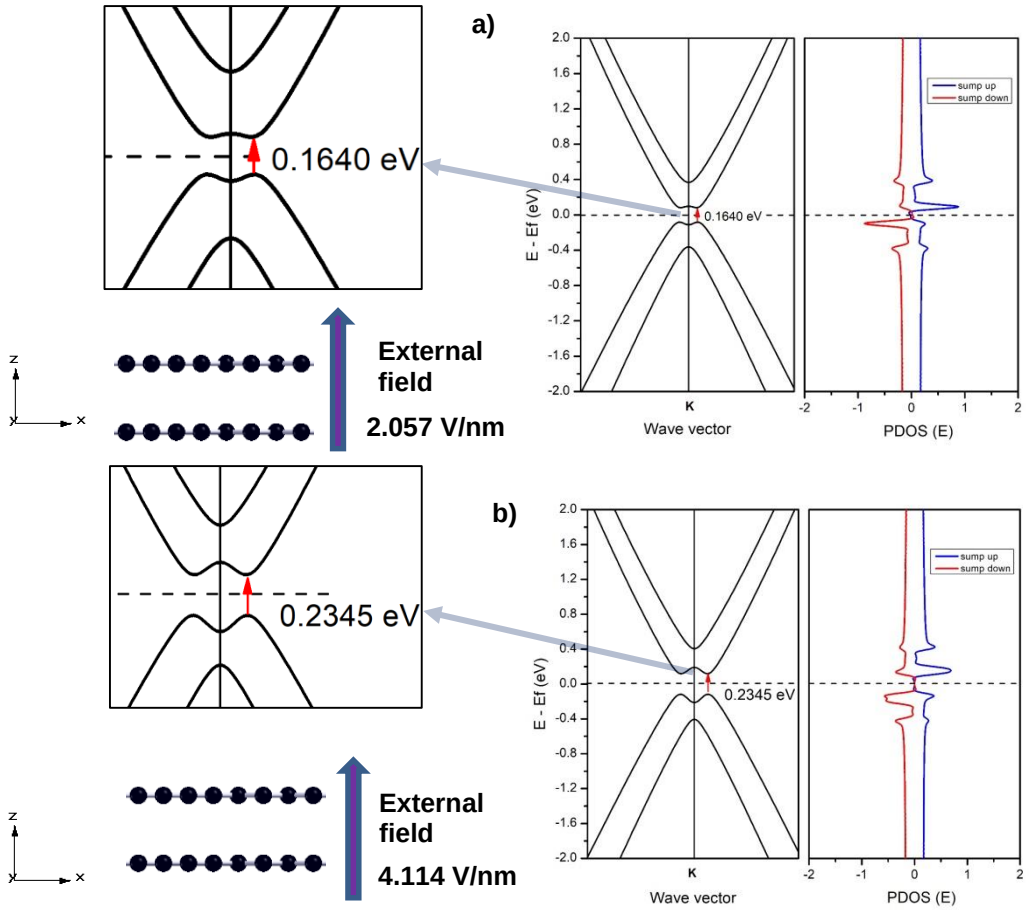

Fig.2. Band structure and PDOS of AB-bilayer graphene with external electric fields *a*) 2.057V/nm and *b*) 4.114 V/nm

To comprehensively investigate the existence of excitons, one can scrutinize the k-resolved density of state (KPDOS) graph for each graphene monolayer and both bilayer layers, as portrayed in Figures 3.a and 3.b. In the absence of an external electric field, electrons occupy states around the Fermi level without creating a band gap. However, upon enforcing an external electric field directed from bottom to top, a band gap is created, as discussed previously. Additionally, the charge density primarily accumulates in the valence bands for the upper graphene monolayer, whereas in the lower layer, the charge concentration is primarily presented in the conduction band. This finding is supportive of the evidence for exciton formation. When an external electric field is applied in the bottom-up direction to AB-bilayer graphene, the previously created exciton comprised of the electron in the upper graphene layer will associate with the hole in the lower graphene layer. Consequently, under the influence of an external electric field, AB-bilayer graphene transforms from its initial metallic state to a semiconductor. Moreover,

the binding energy of excitons increases in response to electric fields, resulting in an expansion of the band gap's width as the electric field intensity increases.

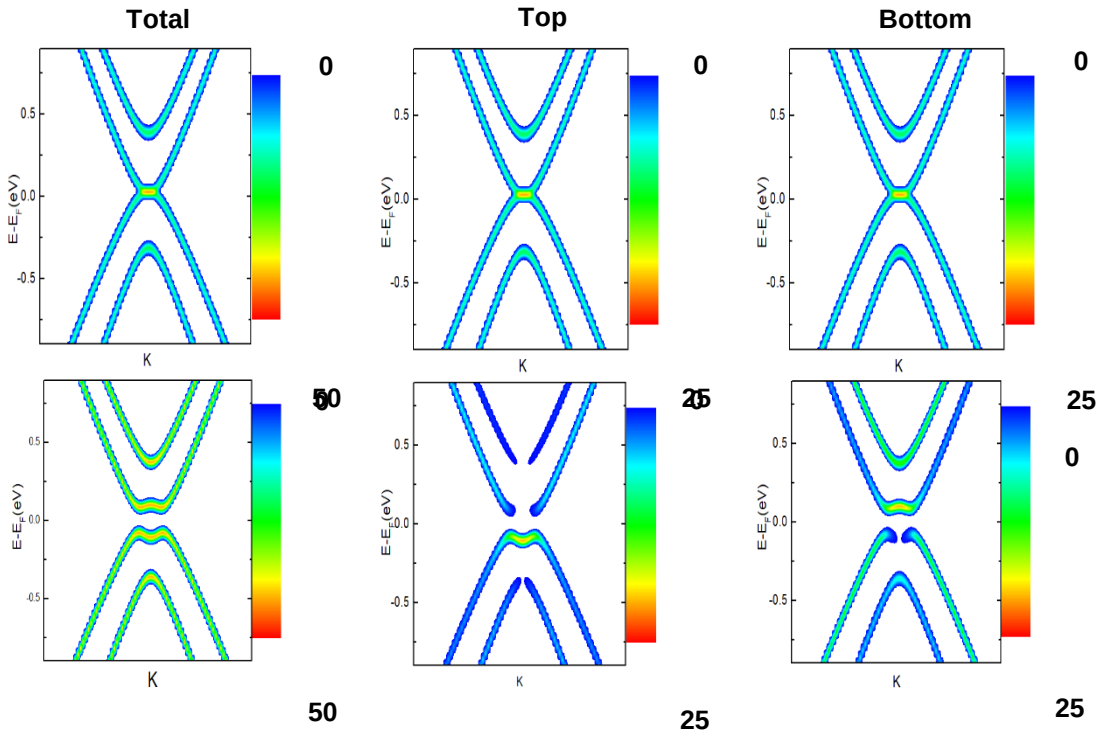

Fig. 3. KPDOS of AB-bilayer graphene *a*) without and *b*) with external electric fields

By analyzing the previously discussed image, we can investigate the impact of charging AB-bilayer graphene under external electric fields. Adjusting the charge density leads to a clear increase in the quantity of electron-hole pairs and, subsequently, changes the band gap. Specifically, doping with additional charges of 0.25% and 0.5% is conducted, and the results are shown in Figure 4.

As the doping concentration of electrons increased, the band gap slightly widened. This occurrence is presented more explicitly in Figure 4.c. However, the change is relatively small, particularly in the case of an electric field intensity of 4.114 V/nm, so it is not yet clear whether increasing the doping concentration will lead to a more significant widening of the band gap. Additionally, Figures 4.*a* and 4.*b* indicate that as the population of doped electrons increases, the Fermi level tends to move upwards toward the conduction band. This trend conforms to semiconductor theory, where adding more negative loads gradually raises the Fermi level (Kittel, 1996).

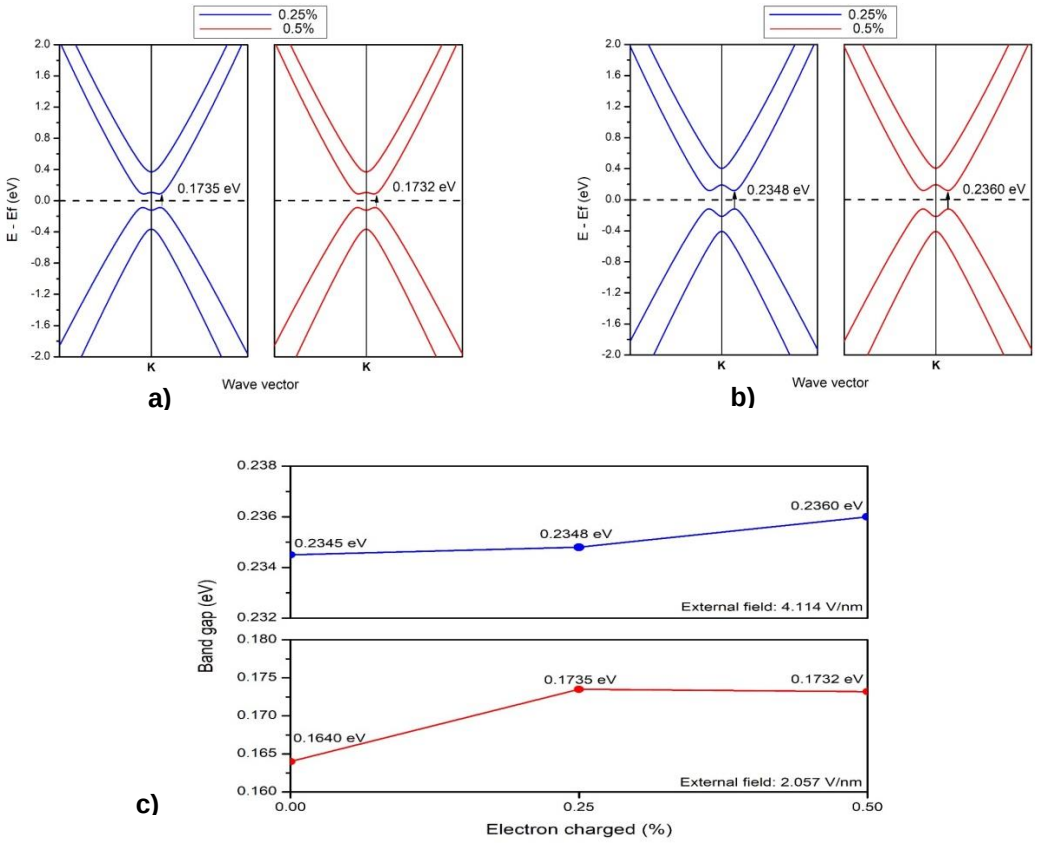

Fig.4. Band structure of AB-bilayer graphene with external electric fields *a*) 2.057 V/nm *b*) 4.114 V/nm with difference charge doping; *c*) the dependence of band gap on charge doping under external electric field 2.057V/nm (up) 4.114 V/nm (down)

3.2. Exciton transitions in hetero-bilayer

The energy band structures of three types of 2D-TMDCs (transition metal dichalcogenides), including MoS_2, $MoSe_2$, and WSe_2, are calculated in their monolayer forms, as demonstrated in Fig. 5. The obtained band gap values for MoS_2, $MoSe_2$, and WSe_2 are 1.7605, 1.4460, and 1.6423 eV, respectively, indicate that all three belong to direct bandgap semiconductor materials, as verified by our simulation results. These outcomes are consistent with previous research studies (Dias *et al.*, 2018; Yun *et al.*, 2012).

We proceed to simulate the AB-stacked bilayer structures for the aforementioned three materials, represented in Fig. 6. The resulting values for MoS_2, $MoSe_2$, and WSe_2 are 0.9109, 1.1867, and 1.3030 eV, respectively, as observed in Fig. 6. A separate research study also conducted the same simulation and published the findings in 2016 (Dybala *et al.*, 2016). Their corresponding results for MoS_2, $MoSe_2$, and WSe_2 were 1.24, 1.20, and 1.23 eV, respectively. Our results for bilayer-AB $MoSe_2$ and bilayer-AB WSe_2 are consistent with their calculations. However, there are considerable discrepancies between the band gap values of our bilayer-AB MoS_2 results (0.9109 eV) and theirs (1.24 eV). However, this result for MoS_2 (1.08 eV) is consistently compared to another study (Zeng *et al.*, 2015).

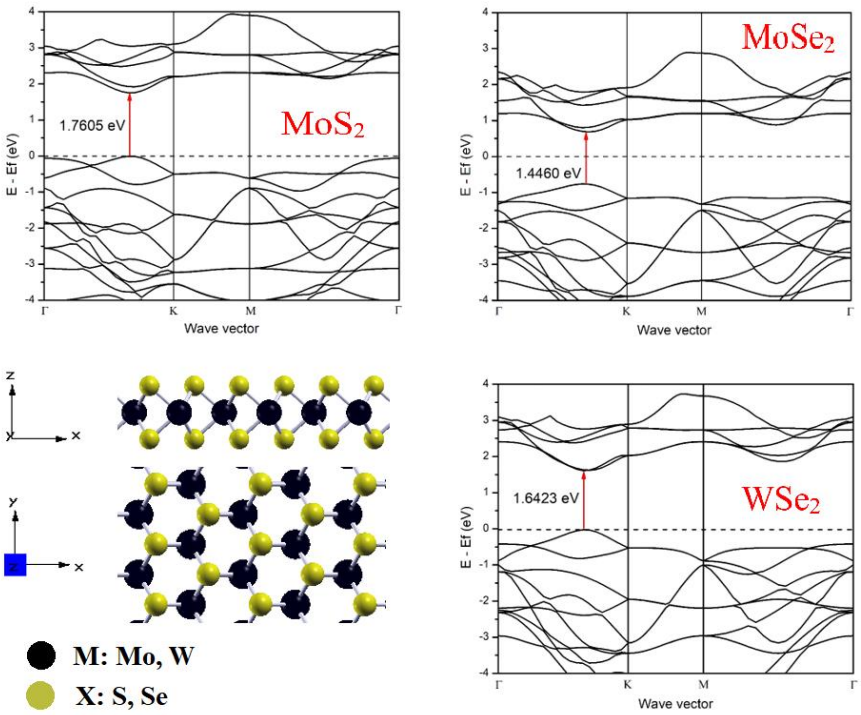

Fig. 5. Band structure of monolayer 2D-TMDCs: MoS_2, $MoSe_2$ and WSe_2

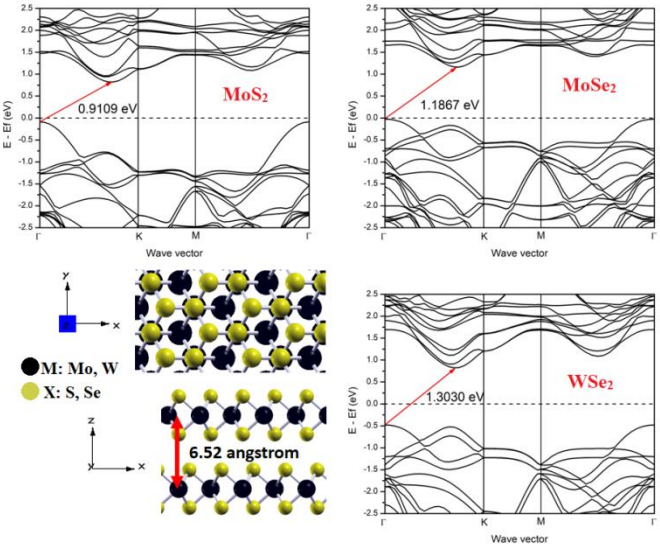

Fig. 6. Band structure of AB-bilayer 2D-TMDCs: MoS_2, $MoSe_2$ and WSe_2

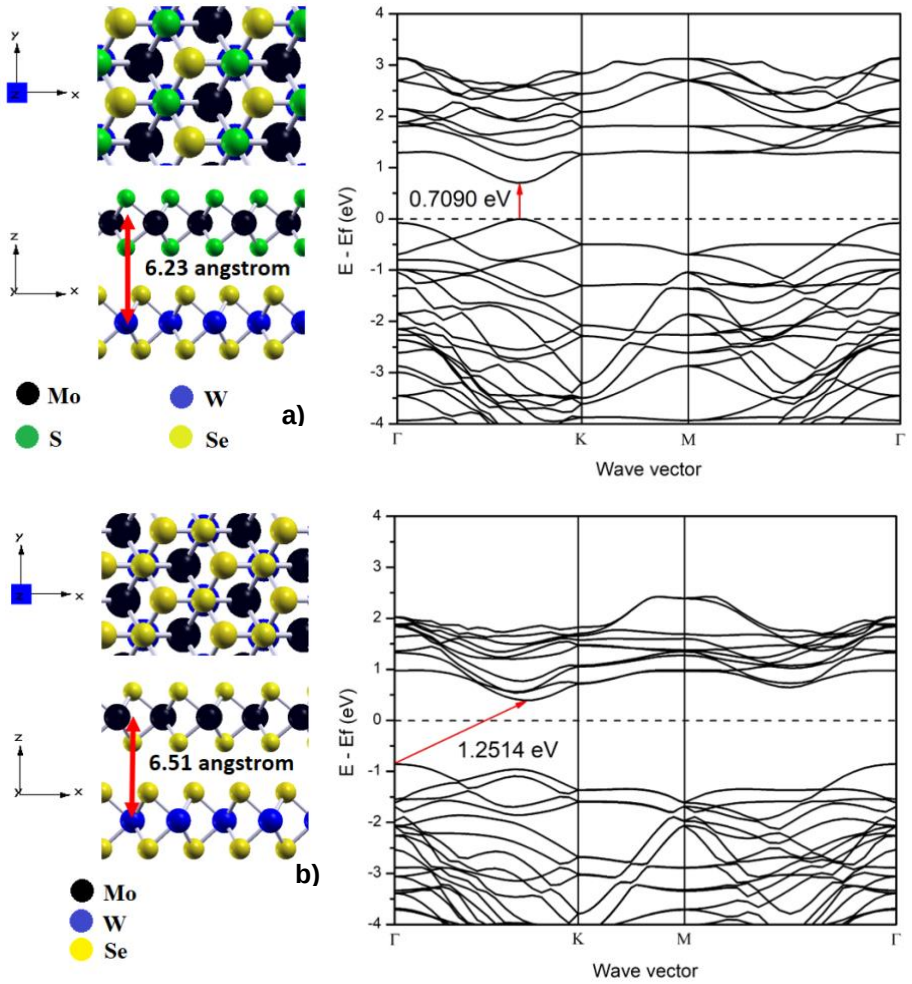

Fig. 7. Crystal structure and band structure of AB-bilayer *a*) MoS_2/WSe_2 and *b*) $MoSe_2/WSe_2$

The aforementioned simulations are homostructures, where both faces of the bilayer are identical, only in a different position. To study the energy level of excitons, we investigate the heterostructure where the upper and lower layers are two different monolayers. Figure 7.*a* shows the calculation result of the AB-bilayer MoS_2/WSe_2 structure simulated by superimposing two different monolayers. This bilayer structure is characterized as a direct semiconductor with a band gap of 0.7090 eV, which is relatively consistent with the calculated results of other research groups (Lu *et al*., 2014; Su *et al*., 2016).

Additionally, it is evident that the band gap value of the bilayer-AB MoS_2/WSe_2 structure is much smaller at 0.7090 eV, as compared to the band gap of each single MoS_2 and WSe_2 monolayer (1.7605 eV and 1.6423 eV, respectively).

We perform simulations of $MoSe_2/WSe_2$ heterostructure bilayers, and the results are presented in Figure 7.b. The simulation results show that the bilayer exhibits indirect characteristics of a semiconductor material with an oblique bandgap of 1.2514 eV. By stacking two monolayers, $MoSe_2$ and WSe_2, in the AB form, the resultant $MoSe_2/WSe_2$ structure displays a reduced band gap, which is consistent with the findings from a different research group (Terrones *et al*., 2013) (which was 1.12 eV). The calculated results presented in Figure 7 confirm the existence of an excitonic transition. These results

imply that combining 2D-TMDCs monolayer heterostructure produces an excitonic transition that reduces the band gap value.

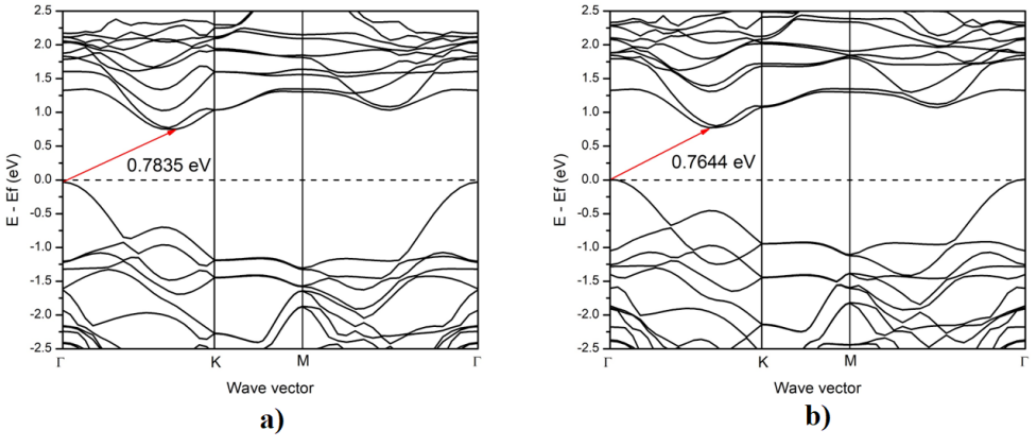

Fig. 8. Band structure of AB-bilayer MoS_2 with external electric field of *a*) 0.5 V/nm and *b*) 1V/nm

In this study, we focus on investigating the effect of external electric fields on the energy structure of bilayer-AB MoS_2 and determining whether it is comparable to that observed in bilayer graphene. We analyze the effect of external electric field values of 0 V/nm (Figure 6), 0.5 V/nm, and 1.0 V/nm (Figure 8) on the bilayer-AB MoS_2. The results indicate that as the external electric field increases, the band gap narrows, reducing from 0.9109 eV in the absence of an electric field to 0.7835 eV when an external electric field of 0.5 V/nm is applied, demonstrating the generation of excitons. Additionally, we observe that applying an external electric field to the bilayer homostructure is a controllable approach that can lead to the formation of heterobilayer pairs. This phenomenon has also been noted in a number of reports (Azhikodan *et al*., 2016; Chu *et al.*, 2015).

4. Conclusion

The coexistence and link between exciton energy levels in multilayer 2-D materials are confirmed in our study. In AB-bilayer graphene, the exciton insulator presents itself in pairs of electronic bonds in the upper layer and holes in the lower layer, particularly upon exposure to an external electric field (or charge doping). The external electric field amplifies the exciton energy level and extends the band gap, thereby offering complete control over the band gap by utilizing of external electric fields and charge doping. In bilayer 2D-TMDC materials, an exciton transition arises when heterostructure bilayer structures are present, producing a reduced band gap compared to that in the homostructure. Moreover, modifying the energy levels of exciton and narrowing the band gap of the material is possible by applying an external electric field to homostructure bilayer materials.

References

Azhikodan, D., Nautiyal, T., Shallcross, S., & Sharma, S. (2016). An anomalous interlayer exciton in MoS_2. *Scientific Reports*, 6(1), 37075.

Blöchl, P.E. (1994). Projector augmented-wave method. *Physical Review B, 50*(24), 17953-17979.

Butov, L.V. (2001). Observation of magnetically induced effective-mass enhancement of quasi-2D excitons. *Physical Review Letters*, *87*(21), 216804.

Chu, T., Ilatikhameneh, H., Klimeck, G., Rahman, R., & Chen, Z. (2015). Electrically tunable bandgaps in bilayer MoS_2. *Nano Letters*, *15*(12), 8000-8007.

Dias, A.C., Qu, F., Azevedo, D.L., & Fu, J. (2018). Band structure of monolayer transition-metal dichalcogenides and topological properties of their nanoribbons: Next-nearest-neighbor hopping. *Physical Review B*, *98*(7), 075202.

Dybała, F., Polak, M.P., Kopaczek, J., Scharoch, P., Wu, K., Tongay, S., & Kudrawiec, R. (2016). Pressure coefficients for direct optical transitions in MoS_2, $MoSe_2$, WS_2, and WSe_2 crystals and semiconductor to metal transitions. *Scientific Reports*, *6*(1), 26663.

Edelstein, W., Spector, H.N., & Marasas, R. (1989). Two-dimensional excitons in magnetic fields. *Physical Review B*, 39, 7697.

Elliott, R.J., Loudon, R. (1960). Theory of the absorption edge semiconductors in a high magnetic. *Journal of Physics and Chemistry of Solids*, 15, 196-207.

Fang, H., Battaglia, C., Carraro, C., & Nemsak, S. (2014). Strong interlayer coupling in van der Waals heterostructures built from single-layer chalcogenides. *Proceedings of the National Academy of Sciences*, *111*(17), 6198-6202.

Frenkel, J.Y. (1931). On the Transformation of Light into Heat in Solids. II. *Physical Review*, *37*(10), 1276-1294.

Giannozzi, P., Baroni, S., Bonini, N., Calandra, M., Car, R., Cavazzoni, C., Ceresoli, D., Chiarotti, G.L., Cococcioni, M. (2009). QUANTUM ESPRESSO: a modular and open-source software project for quantum simulations of materials. *Journal of Physics: Condensed Matter*, 21, 395502.

Kittel, C. (1996). *Introduction to Solid State Physics* (7th ed.). New York: Wiley.

Lu, N., Guo, H., Li, L., Dai, J., Wang, L., Mei, W.-N., & Zeng, X.C. (2014). MoS_2/MX_2 heterobilayers: bandgap engineering via tensile strain or external electrical field. *Nanoscale*, *6*(5), 2879–2886.

Monkhorst, H.J., Pack, J.D. (1976). Special points for Brillouin-Zone integrations. *Physical Review B*, 13, 5188-5192.

Moskalenko, S.A., Snoke, D.W. (2000). Bose-Einstein condensation of excitons and biexcitons and coherent nonlinear optics with excitons. *Cambridge University Press*, 1-9.

Mott, N.F., Littleton, M.J. (1938). Conduction in polar crystals. I. Electrolytic conduction in solid salts. *Transactions of the Faraday Societ*, 34, 485-499.

Palummo, M., Bernardi, M., Grossman, J.C. (2015). Exciton Radiative Lifetimes in Two-Dimensional Transition Metal Dichalcogenides. *Nano Letters*, 15(5), 2794-2800.

Perdew, J.P., Burke, K., & Ernzerhof, M. (1996). Generalized Gradient Approximation Made Simple. *Physics Review Letters*, *77*(18), 3865-3868.

Raza, H., Kan, E.C. (2009). Field modulation in bilayer graphene band structure. *Journal of Physics: Condensed Matter*, *21*(10), 102202.

Sahu, S., Parashar, S.S., & Rout, G.C. (2016). Theoretical study of band gap opening in AB-stacked Bi-layer graphene by impurity and electric field effects. *Materials Today: Proceedings*, *3*(1), 39-44.

Su, X., Ju, W., Zhang, R., Guo, C., Zheng, J., Yong, Y., & Li, X. (2016). Bandgap engineering of MoS_2/MX_2 (MX_2 = WS_2, $MoSe_2$ and WSe_2) heterobilayers subjected to biaxial strain and normal compressive strain. *RSC Advances*, *6*(22), 18319-18325.

Terrones, H., López-Urías, F., & Terrones, M. (2013). Novel hetero-layered materials with tunable direct band gaps by sandwiching different metal disulfides and diselenides. *Scientific Reports*, *3*(1), 1549.

Thonhauser, T., Cooper, V.R., Li, S., Puzder, A., Hyldgaard, P., & Langreth, D.C. (2007). Van der Waals density functional: Self-consistent potential and the nature of the van der Waals bond. *Physical Review B*, *76*(12), 125112.

Torbatian, Z., Asgari, R. (2018). Plasmonic Physics of 2D Crystalline Materials. *Applied Sciences*, *8*(2), 238.

Wang, R.-N., Dong, G.-Y., Wang, S.-F., Fu, G.-S., & Wang, J.-L. (2016). Intra- and inter-layer charge redistribution in biased bilayer graphene. *AIP Advances*, *6*(3), 035213.

Wang, Z., Selbach, S.M., & Grande, T. (2014). Van der Waals density functional study of the energetics of alkali metal intercalation in graphite. *RSC Advances*, *4*(8), 3973-3983.

Wannier, G.H. (1937). The Structure of Electronic Excitation Levels in Insulating Crystals. *Physical Review*, *52*(3), 191-197.

Werdehausen, D., Takayama, T., Albrecht, G., & Lu, Y. (2018). Photo-excited dynamics in the excitonic insulator Ta2NiSe5. *Journal of Physics: Condensed Matter*, 30(30), 305602.

Yun, W.S., Han, S.W., Hong, S.C., Kim, I.G., & Lee, J.D. (2012). Thickness and strain effects on electronic structures of transition metal dichalcogenides: 2H-MX_2 semiconductors (M=Mo, W; X=S, Se, Te). *Physical Review B*, *85*(3), 033305.

Zeng, F., Zhang, W.-B., & Tang, B.-Y. (2015). Electronic structures and elastic properties of monolayer and bilayer transition metal dichalcogenides MX_2 (M = Mo, W; X = O, S, Se, Te): A comparative first-principles study. *Chinese Physics B*, *24*(9), 097103.

Zhen, Z., & Zhu, H. (2018). Graphene: Fabrication, Characterizations, Properties and Applications. *Elsevier Inc.*, 1-12.